Int J Adv Manuf Technol (2007) 32: 932–941
DOI 10.1007/s00170-005-0400-7

ORIGINAL ARTICLE

G. Tsoukantas · K. Salonitis · A. Stournaras · P. Stavropoulos · G. Chryssolouris

On optical design limitations of generalized two-mirror remote beam delivery laser systems: the case of remote welding

Received: 20 May 2005 / Accepted: 23 September 2005 / Published online: 11 April 2006

Abstract Remote welding opens new possibilities for the highly productive and qualitative joining of metal structures, especially in the automotive industry. This work first summarises the different types of remote welding systems (RWSs) based primarily on the different features of the laser beam scanning systems that RWSs implement. A generalised two-mirror scanning system is geometrically analyzed in order to evaluate the irradiated laser intensity on the workpiece as it changes due to the inclinations with which the laser beam impinges to the processing plane. The study discusses the limitations that a two-mirror scanning system enforces in remote welding, and sets the foundation for further theoretical and experimental investigation of this process.

Keywords Laser scanning systems · Remote welding · Remote welding systems · Laser welding · Inclined laser welding

Abbreviations RWS: Remote welding system · N/P: Not possible to initiate keyhole welding, at such conditions, even at normal incidence

Nomenclature

ϕ	the supplementary angle to the laser beam's incidence angle on the processing plane.
ω	the orientation angle of the major semi-axis of the laser's elliptical beam spot on the processing plane.
y_0	the coordinate of the first reflecting mirror's revolution axis along the y axis of the universal coordinate system, {U}.
z_0	the coordinate of the first and the second reflecting mirrors' centres along the z axis of the universal coordinate system, {U}.
c	the minimum allowable distance of the focus lens from the first reflecting mirror.
r_{f_0}	the Gaussian laser beam radius at the focal plane, defined as the beam radius at which the laser intensity has decreased to $1/e^2$ of its maximum value located at the beam's centre.
$r_{f_0}'(\phi)$	the major semi-axis of the laser's elliptical beam spot.
$r_{f_0}''(z_r)$	the laser beam's radius as a function of distance, z_r.
z_r	the distance from the focal plane along the laser beam axis.
M^2	1.2, the laser beam's quality parameter.
λ	10.6 μm, the laser's wavelength.
δ_f	the position of the focal plane in respect to the processing plane. Negative values for δ_f are used for focal planes below the processing plane.
$I(r)$	the laser intensity distribution on a cyclic laser beam spot.
I_0	the maximum laser intensity of the beam on a cyclic laser beam spot.
$I_E(r,\theta)$	the laser intensity distribution on an elliptical laser beam spot.
I_{0_E}	the maximum laser intensity of the beam on an elliptical laser beam spot.
r	the position length of an arbitrary point within a laser beam's spot in respect to the centre of the spot.
θ	position angle of an arbitrary point within a laser beam's spot in respect to the centre of the spot.
r_E	the position length of an arbitrary point of the elliptical beam spot's boundary.
x_E, y_E	the coordinates of an arbitrary point of the elliptical beam spot's boundary.
P	the laser power.
z_{r_0}	the depth of focus.
$I_{keyhole}$	the critical laser intensity to initiate keyhole welding.
u	the welding speed.

G. Tsoukantas · K. Salonitis · A. Stournaras · P. Stavropoulos · G. Chryssolouris (✉)
Laboratory for Manufacturing Systems and Automation, Department of Mechanical Engineering and Aeronautics, University of Patras, Patras, 261 10, Greece
e-mail: xrisol@mech.upatras.gr
Tel.: +30-2610-997262
Fax: +30-2610-997744

1 Introduction

Sheet metal working industries, such as the automotive industry, pose high efficiency and flexibility demands when it comes to joining systems. These demands resulted in the conception [1] and development of remote welding systems (RWSs) [2]. Based on the process of laser welding [3], RWSs integrate a number of sub-systems, including:

1. High-power, high-quality CO_2, Nd:YAG or disk laser sources,
2. Long focal lengths (up to 1.6 m),
3. Rapid *xyz* laser beam scanning/positioning systems (up to 230 m/min, 10 g [4]),
4. Rapid *xy* workpiece moving tables (1 m/min) for large field stations,
5. Robot coupling for small field stations,
6. Off-line programming software for path planning and process parameters selection and
7. Process monitoring systems.

Such configurations generate three-dimensional-shaped working volumes, which may reach nearly 2 m^3 [5] and allow the joining of bulky, three-dimensional components, in multiple processing planes, with minimized positioning times between subsequent welding locations (up to 60 ms for a distance of 100 mm [5]).

A key issue in a RWS is the laser scanning system, which guides the laser beam in the generated working volume. Two basic types of systems have been introduced so far [2, 4–10]. The first type concerns large-field, gantry-type RWSs that use high-power, high-quality CO_2 slab lasers, coupled with a two- or one-mirror scanning systems (Fig. 1). A high-acceleration (10 g) moving device is also implemented in order to translate linearly the focus lens and generate a three-dimensional working volume. Focal lengths in such systems typically range between 1 and 1.6 m. Small-field CO_2 RWSs have also been reported, however, so far with only limited applicability [6, 7].

The second type of RWS involves smaller field stations with two-mirror scanning systems, coupled usually with F-theta optics, which follow the second reflecting mirror for the realisation of a plane image field with small variance in the laser beam incidence (max. variance ca. 6° [7]). Such a configuration is coupled with a robot station and a fibre optic (e.g. 400 μm core diameter) guided, high-quality, diode-pumped Nd:YAG laser [6, 7]. Although the presence of the F-theta optic in the case of a robot RWS considerably restricts the variance of the incidence angle, the kinematics of the robot provides the potential rotation of the whole scanning system with respect to the processing plane, which can result in an angle ϕ of even less than 50°.

An experimental study on 1018 steel with a two-mirrored, large-field, gantry RWS revealed that in inclined welds, the difference between the inline penetration depth (dimension of weld boundaries along the weld axis) and the vertical penetration depth (Fig. 2) is gradually increasing for a reduced laser beam incidence angle, reaching a maximum of 10% of the full penetration depth for the investigated joint [4]. For the case of butt welding, tests on

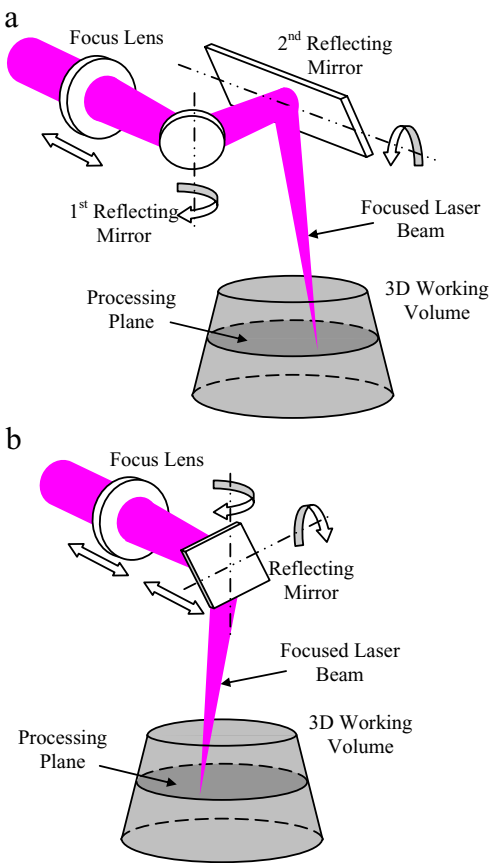

Fig. 1 Principles of scanning systems for remote welding. **a** Two mirrors. **b** One mirror. (schematic not to scale)

3-mm and 0.9-mm-thick sheets, have shown that a maximum offset distance between the sheet metals' edges of 0.4 mm is the boundary to achieve a full-penetration welding. In [7], the major differences met between Nd:YAG (small field) and CO_2 (large field and small field) laser-based RWS and their subcomponents were presented. Issues such as motion axes and optical components, control requirements, path planning and process-simulation software, and requirements for clamping and process monitoring were discussed. Two small-field RWSs, one coupled with a CO_2 slab laser and the other with a diode-pumped Nd:YAG laser were presented. Experimentation with these

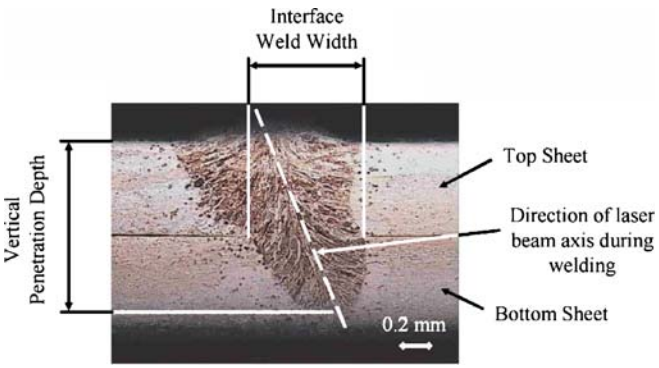

Fig. 2 Cross section of a directional remote-laser lap weld

systems has shown that the presence of the F-theta optic in the Nd:YAG-based system was beneficial in terms of welding penetration depth reduction (up to 55%).

The operating principle of a scanning system introduced by a RWS implies that the laser beam impinges onto the material's surface with different inclinations. This leads to elliptical beam spot areas, distorted laser intensity distribution, and lower laser intensity, with respect to normal incidence. Since the keyhole formation mechanism requires a specific material, for a critical laser intensity, I_{keyhole}, in order to induce material vaporisation [11, 12], the inclinations of the laser beam primarily affect the keyhole initiation, and if achieved, the resulting keyhole and molten pool shape as well. Keyhole formation allows the laser beam to intrude into the materials' mass along the direction of impingement and transfer its energy to a deeper region of the workpiece with respect to conduction welding where no vaporisation occurs. Thus, the laser beam inclinations also affect the directionality of the keyhole cavity and, consequently, the direction that melting and joining occur.

This study investigates the geometrical and optical limitations of a generalised two-mirror scanning system and the way that these are reflected on the case of remote welding. The presented geometrical analysis is generalised and can be potentially applied to all processes in which such scanning systems have been utilised (e.g. stereolithography, 3D digitizing,), however, remote welding is chosen as the process that is most affected by the optical limitations of the scanning system: i.e. extreme inclination, results in laser intensities below the critical laser intensity, I_{keyhole}, under which joining is not possible at all, especially when lap joints are performed (e.g. automotive, application). The presented analysis can be utilized for the development of scanning systems for remote welding (and other processes) instead of costly and time-consuming trial-and-error methods that have been used extensively so far, as part of the development of RWSs. The parameterized geometrical measures provided are necessary for the development of process modelling of remote welding [13], which is of major importance considering the industrial potential of this new process and the consequent requirements of off-line programming (i.e. process parameters' selection) and process monitoring and control.

The study also discusses the effects that the particularity of the laser inclinations introduce to conventional laser welding and presents welding angle limitations on different materials, using a typical large-field RWS with a two-mirror scanning system as an example.

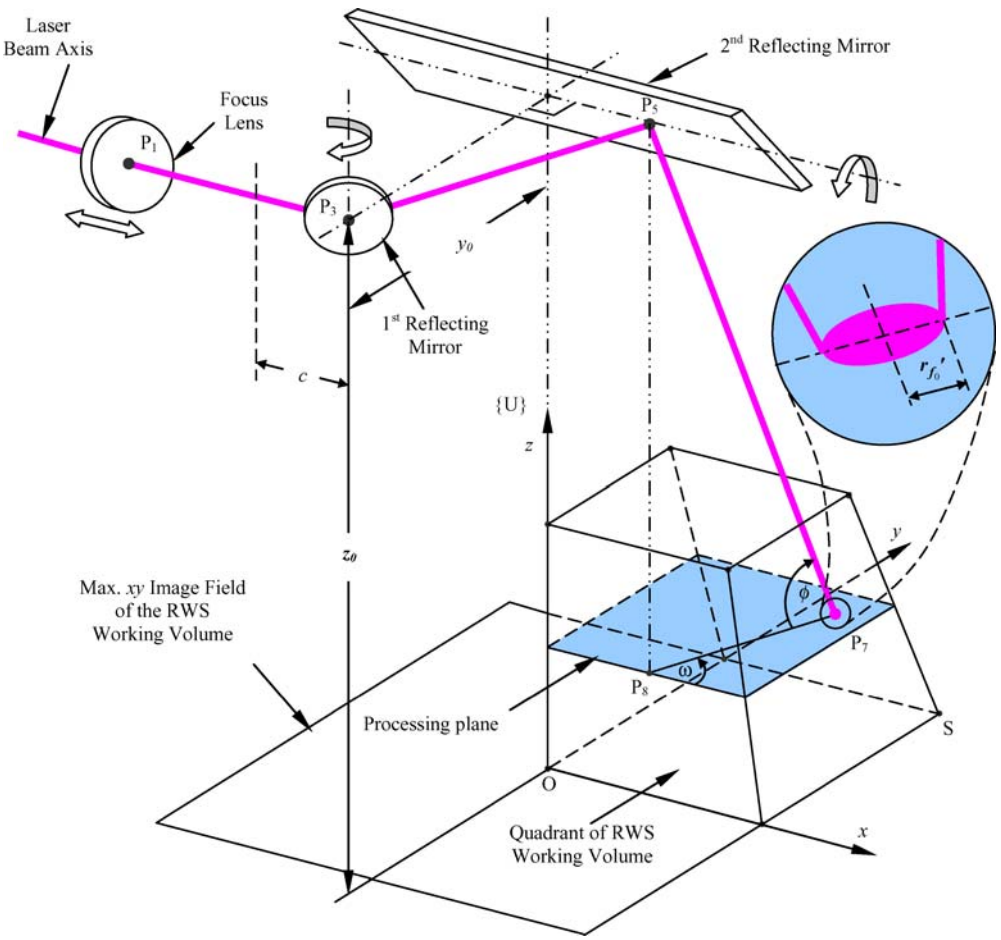

Fig. 3 Typical RWS with a two-mirror scanning system (schematic is not to scale)

2 Geometrical analysis of a two-mirror RWS scanning system

A typical RWS that implements a two-mirror scanning system provides the mirrors' rotation about two vertical (skew) axes. The focus lens seats on a stage that can be linearly translated so as to provide a three-dimensional working volume (Fig. 3). The laser beam can impinge onto a horizontal processing plane with a normal incidence, only to the points that belong to the z-axis of the universal coordinate system of Fig. 3. In any other location, the beam's incidence (angle ϕ) is less than 90°.

In any case of inclination, the beam's spot is only distorted along the direction of the linear segment (P_8P_7). Although a constant horizontal processing plane is not met exclusively in real-life applications, the investigation of this case is considered as a reference for the geometrical analysis of a scanning system and the effects it introduces during welding.

The dynamical behaviour of remote welding is enhanced by the fact that not only the incidence but also the orientation (angle ω in Fig. 3) of the elliptical beam spots', varies from point to point. This orientation remains constant along a seam whose trajectory lies on the x or y axes. Such trajectories are also not used exclusively in real-life applications, but they can be used to ease the RWS's and the investigation of the process (Fig. 4).

In order to evaluate the effects that the laser beam inclinations introduce, and to study the limitations of RWSs, the geometrical analysis of the implemented scanning system is performed (see Appendix). The analysis derives analytical expressions of the angle, ϕ, and the orientation angle, ω, of the elliptical beam spots' major semi-axis. Through this analysis the major semi-axis, r'_{f_0}, of the beam spots and the laser's intensity distribution, $I_E(r;\theta)$, are calculated as functions of the co-ordinates of the laser beam's centre, P_7, on the processing plane.

Although the RWSs presented so far pose quite simple construction with rotating mirrors about only two vertical axes and a steady laser source (Fig. 3), the analysis presented in the Appendix considers a more generalised case where:

1. The laser direction towards the first reflecting mirror can be altered, and
2. The second reflecting mirror can be rotated about three vertical axes, which provide an arbitrary orientation of this reflecting mirror in space.

The generality of the problem is also enhanced by the fact that an arbitrary oriented processing plane is considered.

Despite the fact that the presented analysis is dedicated to two-mirror scanning systems of large- or small-field RWSs, in its simplified form it can be applied to:

1. RWSs that implement one-mirror scanning systems, and
2. small-field RWSs that implement F-theta optics, usually after the second reflecting mirror.

In order to produce the equations of case (1), the analysis is simplified by eliminating the rotation of the first scanning mirror and by eliminating the rotation of the second scanning mirror about the axis y'''. For the case (2), the presented analysis is supplemented by the ratio of the incidence angle in the input over the angle, on the output window of the F-theta optics, a factor that is provided by the F-theta optics manufacturer. Since in a small-field RWS the scanning head is coupled with a robot arm, the robot kinematics also has to be considered in order to derive the final incidence and orientation angles provided by the presented analysis.

Considering the angles ϕ, ω, as given from the geometrical analysis, the major semi-axis of the elliptical beam spot is provided:

$$r'_{f_0} = \frac{z_r}{\cos\phi} \tag{1}$$

The laser beam radius, $r_{f_0}{}''$, as a function of distance, z_r, from the focal plane is provided by the following equations:

$$r_{f_0}{}'' = z_r \tan\phi \tag{2}$$

$$r_{f_0}(z_r) = r_{f_0}\left[1 + \left(M^2\frac{\lambda(z_r+\delta_f)}{\pi r_{f_0}^2}\right)^2\right]^{1/2} \tag{3}$$

By solving Eqs. (2), (3) for δ_f=0, distance z_r is calculated, which plugged into Eq. (1) derives the major semi-axis of the elliptical beam spot:

$$r'_{f_0}(\phi) = \frac{r_{f_0}}{\cos\phi\cdot\sqrt{\tan^2\phi - \left(\frac{M^2\lambda}{\pi r_{f_0}}\right)^2}} \tag{4}$$

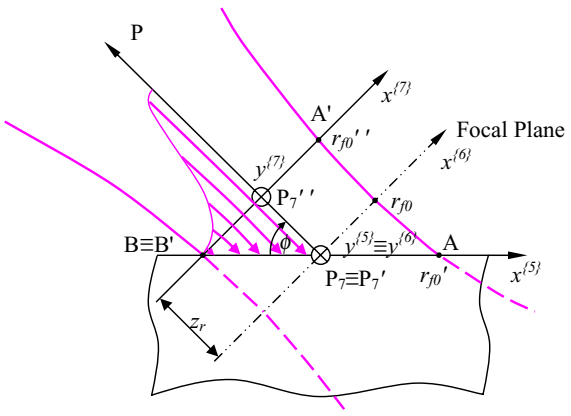

Fig. 4 Radius of an inclined laser beam at depth z_r from the focal plane

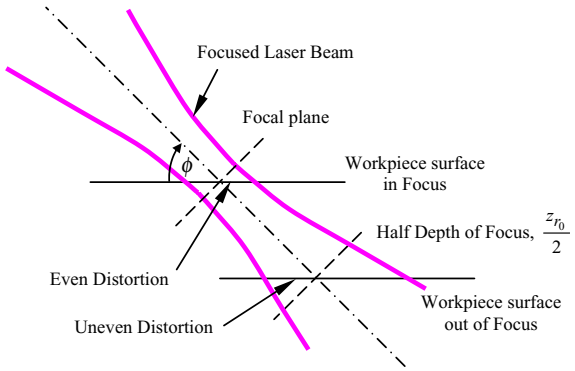

Fig. 5 Even and uneven distortion of laser intensity

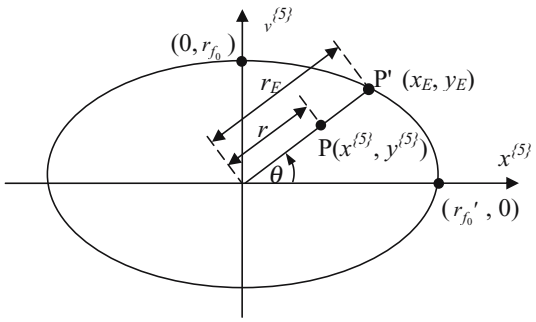

Fig. 6 Elliptical beam spot

3 Laser beam intensity distribution

The Gaussian laser beam intensity distribution for a cyclic laser beam spot is:

$$I(r) = I_0 \exp\left(\frac{-2r^2}{r_{f_\phi}''^2}\right) \tag{5}$$

The maximum intensity of the beam, I_0, is calculated from the total laser beam power, P:

$$P = 4\int_0^{\frac{\pi}{2}}\int_0^{\infty} I_0 \exp\left(\frac{-2r^2}{r_{f_\phi}''^2}\right) r dr d\theta = \frac{\pi r_{f_\phi}''^2}{2} I_0 \tag{6}$$

Due to the elliptical beam spots that are formed from the inclined incidence of the laser beam onto the material, the Gaussian laser beam intensity profile differs from the one of Eq. (5). An absolute even distortion of the beam's intensity is achieved when the focal point lies onto the workpiece (see Fig. 5). In any other case the distortion is uneven, producing maximums and minimums within the elliptical spot.

In real-life applications, such a condition is possible with the application of autofocus systems. Thus, it can be assumed that while the processing plane will be within the range defined by the depth of focus, no major laser intensity unevenness will be posed at the workpiece. This is justified by the fact that the depth of focus in a RWS, is relatively higher in respect to conventional welding systems, due to the longer focal length (see Table 1).

Following the basic form of Eq. (5), the laser intensity distribution on an elliptical beam spot will be:

$$I_E = I_{0_E} \exp\left[\frac{-2\left(x^{\{5\}^2} + y^{\{5\}^2}\right)}{(x_E^2 + y_E^2)}\right] = I_{0_E} \exp\left(\frac{-2r^2}{r_E^2}\right) \tag{7}$$

By using the polar coordinates and the general ellipse equation, the following relation occurs:

$$r_E^2 = \frac{r_{f_0}'^2 r_{f_0}^2}{r_{f_0}^2 \cos^2\theta + r_{f_0}'^2 \sin^2\theta} \tag{8}$$

Thus, the laser intensity profile on the elliptical spot will be:

$$I_E(r,\theta) = I_{0_E} \exp\left[\frac{-2r^2\left(r_{f_0}^2 \cos^2\theta + r_{f_0}'^2 \sin^2\theta\right)}{r_{f_0}'^2 r_{f_0}^2}\right] \tag{9}$$

The maximum intensity of the beam, I_{0_E}, is calculated from the total laser beam power, P:

$$P = 4\int_0^{\frac{\pi}{2}}\int_0^{\infty} I_{0_E} \exp\left[\frac{-2r^2\left(r_{f_0}^2 \cos^2\theta + r_{f_0}'^2 \sin^2\theta\right)}{r_{f_0}'^2 r_{f_0}^2}\right] r dr d\theta$$
$$= \frac{\pi r_{f_0}' r_{f_0}}{2} I_{0_E} \tag{10}$$

Equations (5), (6) are provided by Eqs. (9), (10) for $r_{f_0} = r_{f_0}'$ (the case of a circular beam spot) (Fig. 6).

Table 1 Properties of laser beam and scanning system for different focal lengths

Focal length (mm)	r_{f_0} (μm)	Depth of focus (mm)	z_{r_0} (mm)	y_0 (mm)	c (mm)	Max. working volume image field $x \times y$ (mm^2)
1,000	182	6	627	127	159	582×425
1,240	210	7.5	727	127	159	974×833
1,600	267	10	1,111	127	159	1,190×826

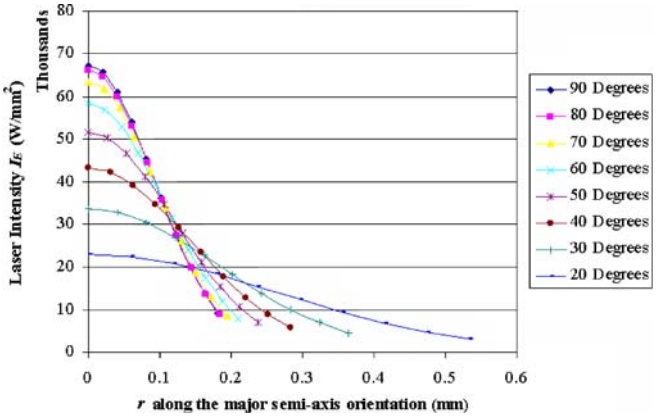

Fig. 7 Laser Intensity profile for different ϕ angles

The calculated laser intensity distribution is presented in Fig. 7 for various ϕ angles along the major semi-axis of the elliptical beam spots that are formed.

4 Application of the analysis on a large-field CO_2 RWS

For the application of the presented study, a prototype large-field RWS as shown in Fig. 3, coupled with a CO_2 slab laser of 3.5 kW nominal output was utilised. Due to the relatively long focal lengths (1–1.6 m), a magnification of two is utilised prior to focusing, in order to provide typical beam spots at the focal plane for laser keyhole welding.

As a typical example, the case of the 1,000-mm focal length at the processing plane z=0 is presented. The maximum laser intensity variation is also calculated within the formed working volume for three different cases of focal length (Figs. 8, 9, 10, 11).

Table 2 provides the minimum ϕ angles and other characteristics of the investigated RWS that can be achieved for the three different focal lengths, considering a horizontal processing plane. The angle values are calculated in the most distant corner (point S on Fig. 3) of the working volume quadrant, considering as limit the laser beam path to be, at the most, equal to the applied focal length.

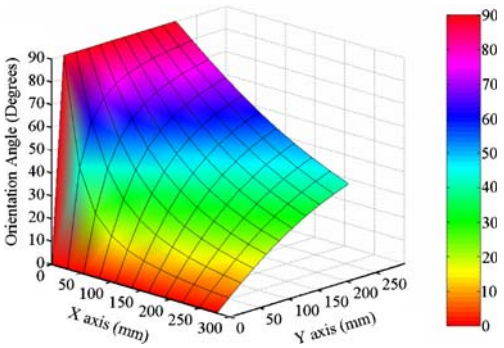

Fig. 9 Orientation angle for a 1,000-mm focal length

5 Remote welding limitations of a large-field CO_2 RWS

In order to calculate the minimum angle ϕ at which welding is possible with the referred RWS, the critical laser intensity required to initiate the keyhole welding, I_{keyhole}, of different materials was used, from the data referred to mainly in [11] and from the authors' work with a large field CO_2 RWS. All referenced data has resulted from the application of CW, CO_2 laser sources for typical production welding speeds, at normal laser beam incidence and with beam spots varying between 80–250 μm.

The values of I_{keyhole} in Table 3, do not refer to the actual laser power absorbed by the material, but to the maximum, nominal laser power output. Moreover, in the calculations of the inclinations no loss of power absorption from the material has been taken into consideration, due to the beam inclination, as stated in [4]. Thus, the presented minimum angle figures may pose a slight underestimation, which according to data from [4], cannot be greater than 10% for angles $\phi \geq 40°$.

Despite the fact that some angle limits of Table 3 are lower than the minimum ϕ angles achieved by the RWS at a horizontal processing plane (Table 2), the angle limits of Table 3 could be used (e.g. for off-line programming reasons) for cases where the processing plane is not horizontal, thus lower values than the ones of Table 2 could be reached. It should be noted that although in some cases the minimum ϕ angles at which keyhole welding can be initiated are quite low (less than 40°), the vertical penetration achieved will be lower than the one referred

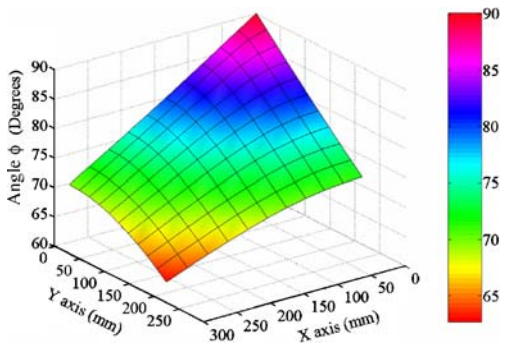

Fig. 8 Angle ϕ for a 1,000-mm focal length

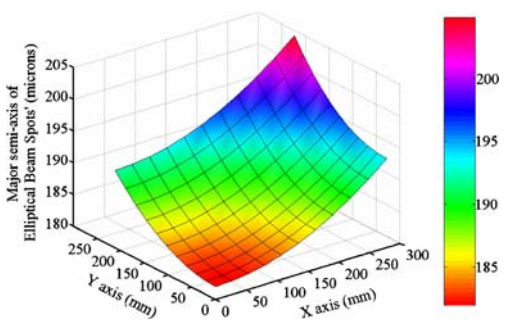

Fig. 10 Major semi-axis of the elliptical beam spots' for a 1,000-mm focal length

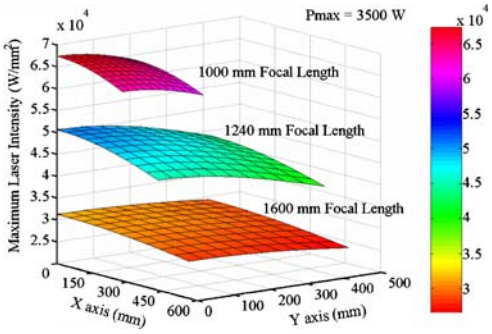

Fig. 11 Maximum laser intensity for three focal lengths

to in Table 3, a fact that in production applications would require lower welding speeds and/or repositioning of the workpiece inside the working volume, so as to achieve greater angle ϕ, consequently greater vertical penetration.

6 Conclusions

This study discusses the particularities and limitations presented by two-mirror scanning systems as they are reflected upon RWSs and on the process itself. For this reason, the geometrical analysis of a generalised two-mirror scanning system was realised and the different geometrical parameters were calculated in order to derive the laser intensity distribution for the different incidences of the laser beam within the formed working volume. Based on this analysis and on experimental data, the minimum angle ϕ limits to which laser keyhole welding is possible were calculated for different materials, information which is necessary for the off-line programming of a RWS but also for any further detailed theoretical and experimental investigation of the process. The main results of this study can be summarised as follows:

- The application of the geometrical analysis on a typical large-field RWS have revealed that depending on the focal length applied, ϕ angles of down to approx. 50° can be formed between the laser beam axis and a horizontal (to the universal coordinate system) processing plane. At such an incidence, the beam spot's radius is stretched by approx. 30%, forming an elliptical spot in which the maximum laser intensity is decreased approx. by 22.5% compared to the intensity achieved at normal incidence. Naturally, lower incidences are possible, inducing much lower maximum laser intensities (Fig. 7) at non-horizontal processing planes, however, the keyhole initiation and if achieved, the penetration efficiency, are questionable (Table 3).
- Depending upon the focal length and the trajectory orientation of a certain seam weld, the incidence for a typical 30-mm seam weld, poses a variance of approx. 2–3°. The beam spot's orientation can vary by more than 40° near the region of the origin of the universal coordinate system falling down to 3° at the working volume's corner points along a typical 30-mm seam weld. Such a phenomenon contributes to the dynamic behaviour of the process and is anticipated to affect the weld width for great variances within a certain seam.
- The maximum laser intensity decreases for decreasing ϕ angles, more steeply at shorter focal lengths since the same incidences for increasing focal lengths are achieved at greater distances from the origin of the universal coordinate system.
- Although some of the non-possible welding cases of Table 3 could be realised with lower welding speeds or/and lower focal lengths, such a fact is in contrast with the industry's continuous requirements for increasing productivity (referring to processing and non-processing times) and flexibility (greater focal lengths), necessitating the development of even higher laser power outputs with advanced quality, suitable for remote welding applications.

Acknowledgement The reported work was partially supported by the project: G1RD-2000-00332, "Highly Efficient & Flexible Remote Welding Systems for Advanced Welded Structures-REMOWELD".

Appendix

The geometrical analysis of a two-mirror scanning system is based on the rotation of the reflecting mirrors' planes (E_1, E_2) and on the laser beam's axis about the axes of local coordinate systems parallel to the universal Cartesian coordinate system {U}: O*xyz* (Fig. 4). The determination of the laser beam's axis direction, due to the interference of the two reflecting mirrors and the angle ϕ on the processing plane, are calculated through the law of reflection.

Table 2 Calculated characteristics at point S and their deviations against point O

Focal length (mm)	Min. φ (Degrees)	Dev. of φ (%)	$r_{f_0}\prime$ (μm)	Dev. of $r_{f_0}\prime$ (%)	Max. laser intensity (10^4 W/mm^2)	Dev. of max. laser intensity (%)
1,000	62.7	−30.33	205	12.53	5.978	−11.1
1,240	50.7	−43.67	271	29.23	3.910	−22.6
1,600	58.6	−34.89	313	17.16	2.668	−14.6

Table 3 Minimum ϕ angles to initiate keyhole welding for different focal lengths

Material type	u (m/min)	$I_{keyhole}$ (10^4 W/mm^2)	Penetration at normal incidence (mm)	Minimum angle ϕ to initiate keyhole welding (degrees)		
				Focal length 1,000 mm	Focal length 1,240 mm	Focal length 1,600 mm
Mild steel [11]	7.5	2.1	0.8	18	25	42
DC04 ($FePO_4$) steel	4	2.9	1	25	35	67
Zinc-coated 600DP high-strength steel	2	3.9	1.6	35	50	N/P[a]
Mild steel 1018 [4]	2	1.2	1	14	18	31
AISI 304 stainless	5	4.0	1.2	37	53	N/P
12SR stainless [11]	1.3	1.5	2	13	17	29
Aluminium 1100 [11]	1	3.1	1	27	38	83
Aluminium 2017 [11]	1	2.7	1	24	32	60
Aluminium 2024 [11]	7.8	4.7	1	44	68	N/P
Aluminium 7N01 [11]	1	2.9	1	26	35	68
Aluminium 5083 [11]	1	2.3	1	20	27	47
Aluminium 5182 [11]	7.8	4.7	1	44	68	N/P
Aluminium 5000× [11]	5	3.5	1	31	44	N/P
Aluminium 5754 [11]	4	2.8	1.5	25	34	64
Aluminium 6000× [11]	5	2.0	1	17	23	40
Aluminium 6016 [11]	6	3.7	1	33	47	N/P
Aluminium 6082 [11]	7.8	4.7	1	44	68	N/P
Copper [11]	5	5.2	1	51	N/P	N/P
Vanadium [11]	7.5	3.2	1	28	39	N/P

[a]N/P: Not possible to initiate keyhole welding, at such conditions, even at normal incidence

Four local Cartesian coordinate systems are defined, $\{A\}: P_1x'y'z'$, $\{B\}: Qx''y''z''$, $\{C\}: Rx'''y'''z'''$, $\{D\}: P_8x^{\{4\}}y^{\{4\}}z^{\{4\}}$ as parallel to, and distant from {U} along distances x_{rl}, y_{rl}, z_{rl}, where l=A-D, respectively. All local coordinate systems are steady, except for {D}, whose location depends on the trace of point, P_5, on the processing plane, E_3. To simplify the analysis, the initial positions of points that define the reflecting planes E_1, E_2 are chosen to belong to the x'' z'' and x''' z''' planes of {B} and {C} respectively. The laser beam axis is defined by the known points $P_1(x_{P_1}, y_{P_1}, z_{P_1})$, $P_2'(x'_{P_2}, y'_{P_2}, z'_{P_2})$ that belong to the x′ axis of {A}. Linear segment (P_1P_2') can be rotated about the z' axis of {A} at angle $\Delta\theta_A$, and is reflected at point P_3 in the first reflecting mirror plane. Plane E_1 can be rotated about the z'' axis of {B} at angle $\Delta\theta_B$, to form a new plane E_1', which reflects the laser beam axis towards the second reflecting mirror plane, at point P_5. Plane E_2 can be rotated about axes x''', z''',y''' of {C} at angles $\Delta\theta_{Cx'''}$, $\Delta\theta_{Cz'''}$ and $\Delta\theta_{Cy'''}$ respectively, to form a new plane E_2'. After the second reflection, the laser beam axis impinges on the processing plane, E_3, at point, P_7, with an angle, ϕ, and an orientation angle, ω, as shown in Fig. 12.

1. Each of the three planes E_i, i = 1–3 is defined at {U} by the triad of points: $X_{i+j}^{\{U\}}(x_{i+j}, y_{i+j}, z_{i+j})$, $X_{(i+j+1)}^{\{U\}}(x_{(i+j+1)}, y_{(i+j+1)}, z_{(i+j+1)})$ and $X_{(i+j+2)}^{\{U\}}(x_{(i+j+2)}, y_{(i+j+2)}, z_{(i+j+2)})$, for the three respective combinations of i, j: $i = 1$ and $j = 0$, $i = 2$ and $j = 2$, $i = 3$ and $j = 4$:

$$E_i: \begin{vmatrix} x & y & z & 1 \\ x_{i+j} & y_{i+j} & z_{i+j} & 1 \\ x_{(i+j+1)} & y_{(i+j+1)} & z_{(i+j+1)} & 1 \\ x_{(i+j+2)} & y_{(i+j+2)} & z_{(i+j+2)} & 1 \end{vmatrix} = 0 \quad (11)$$

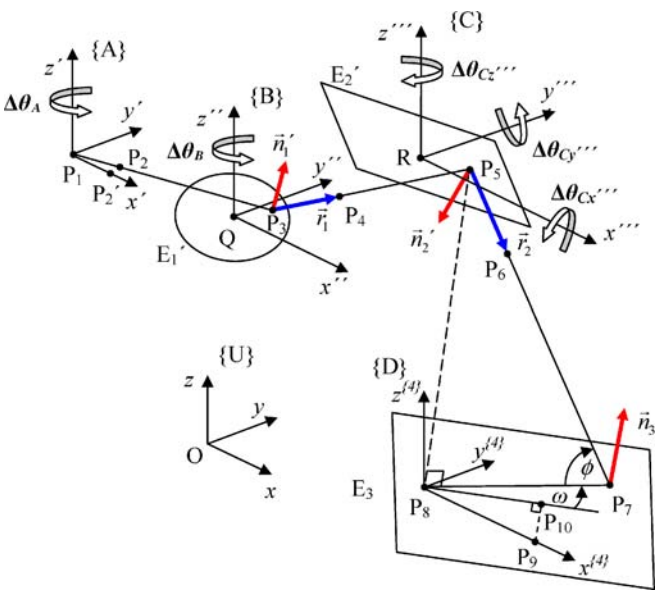

Fig. 12 Geometrical analysis of the RWS scanning system

which concludes to the general plane equations, for i = 1–3:

$$E_i : a_i x + b_i y + c_i z + d_i = 0 \tag{12}$$

2. The rotation of linear segment P_1P_2' about the z' axis of {A} at an angle $\Delta\theta_A$, results to a new point, P_2, which position vector, ${}^U\overrightarrow{p}_{P_2}$, at {U} is provided, by the following relations, for, $l = A$, $m = P_2$, $z = z'$, and $n = P_2'$:

$${}^U\overrightarrow{p}_m = {}^U Trans_l \cdot {}^l Rot_z \cdot \left({}^U Trans_l\right)^{-1} \cdot {}^U\overrightarrow{p}_n \tag{13}$$

where ${}^U Trans_l$ is the transformation matrix of coordinate system $\{l\}$, in respect to the universal coordinate system {U}:

$${}^U Trans_l = \begin{bmatrix} 1 & 0 & 0 & x_{rl} \\ 0 & 1 & 0 & y_{rl} \\ 0 & 0 & 1 & z_{rl} \\ 0 & 0 & 0 & 1 \end{bmatrix} \tag{14}$$

and ${}^l Rot_z$ is the rotation matrix about the z axis of coordinate system $\{l\}$, at angle $\Delta\theta_l$:

$${}^l Rot_z = \begin{bmatrix} \cos\Delta\theta_l & -\sin\Delta\theta_l & 0 & 0 \\ \sin\Delta\theta_l & \cos\Delta\theta_l & 0 & 0 \\ 0 & 0 & 1 & 0 \\ 0 & 0 & 0 & 1 \end{bmatrix} \tag{15}$$

3. The rotation of plane E_1 and its defining points $X_i^{\{U\}}$, i = 1–3 about the z'' axis of {B} at an angle $\Delta\theta_B$, results to a new triad of points $X_i^{\{U\}'}\left(x_i', y_i', z_i'\right)$, $X_{(i+1)}^{\{U\}'}\left(x'_{(i+1)}, y'_{(i+1)}, z'_{(i+1)}\right)$ and $X_{(i+2)}^{\{U\}'}\left(x'_{(i+2)}, y'_{(i+2)}, z'_{(i+2)}\right), i = 1$ which define the new reflecting plane, E_1'. The position vectors of the resulting points of plane E_1' are calculated by Eqs. (13), (14), (15), for l=B, m=$X_i^{\{U\}}{}'$, z=z'', n = $X_i^{\{U\}}$ and i=1–3. According to Eq. (11), for x_i=x_i', y_i=y_i', z_i=z_i' with i=1–3, the plane equation of E_1' is defined, which results to the following general form, for i=1:

$$E_i' : a_i' x + b_i' y + c_i' z + d_i' = 0 \tag{16}$$

4. The laser beam axis represented by the linear segment (P_1P_2) impinges on plane E_1' at point P_3. The position vector of point P_3, ${}^U\overrightarrow{p}_{P_3}$, is derived by the solution of the following relations, for i=1, j=1 and k=1:

$${}^U\overrightarrow{p}_{P(i+2)} = {}^U\overrightarrow{p}_{Pi} + \left({}^U\overrightarrow{p}_{Pi} - {}^U\overrightarrow{p}_{P(i+1)}\right) t_j \tag{17}$$

where

$$t_j = \frac{\begin{vmatrix} 1 & 1 & 1 & 1 \\ x_k' & x'_{(k+1)} & x'_{(k+2)} & x_{P_i} \\ y_k' & y'_{(k+1)} & y'_{(k+2)} & y_{P_i} \\ z_k' & z'_{(k+1)} & z'_{(k+2)} & z_{P_i} \end{vmatrix}}{\begin{vmatrix} 1 & 1 & 1 & 1 \\ x_k' & x'_{(k+1)} & x'_{(k+2)} & x_{P_{(i+1)}} - x_{P_i} \\ y_k' & y'_{(k+1)} & y'_{(k+2)} & y_{P_{(i+1)}} - y_{P_i} \\ z_k' & z'_{(k+1)} & z'_{(k+2)} & z_{P_{(i+1)}} - z_{P_i} \end{vmatrix}} \tag{18}$$

5. The impinging point, P_5, of the laser beam axis on the second reflecting plane, is calculated through the position vector of point P_4 that belongs to the reflecting vector, $\overrightarrow{r_1}$. Point P_4 is provided by the unit vector $\hat{n}_1'$ of the normal vector $\overrightarrow{n}_1' = \left[a_1' \; b_1' \; c_1'\right]^T$, for i = 1 and j = 1:

$$\begin{aligned} {}^U\overrightarrow{p}_{P_{(i+3)}} &= \overrightarrow{r}_j + {}^U\overrightarrow{p}_{P_{(i+2)}} \\ &= \overrightarrow{P_iP}_{(i+2)} - 2\left(\overrightarrow{P_iP}_{(i+2)} \cdot \hat{n}_j'\right) \cdot \hat{n}_j' \end{aligned} \tag{19}$$

6. The sequential rotation of plane E_2 and its defining points $X_i^{\{U\}}$, i=4–6 about the x''', z''', y''' axes of {C} at angles $\Delta\theta_{Cx'''}$, $\Delta\theta_{Cz'''}$ and $\Delta\theta_{Cy'''}$ respectively, result in a new triad of points $X_i^{\{U\}}{}'$, $\left(x_i', y_i', z_i'\right)$, $X_{(i+1)}^{\{U\}}\left(x'_{(i+1)}, y'_{(i+1)}, z'_{(i+1)}\right)$ and $X_{(i+2)}^{\{U\}}{}'$, $\left(x'_{(i+2)}, y'_{(i+2)}, z'_{(i+2)}\right)$, i= 4, which define the new reflecting plane, E_2'. The position vectors of the resulting points of plane E_2' are calculated by Eqs. (13) and (14), for l=C, m=$X_i^{\{U\}}{}'$, z=$x'''z'''$ y''', n = $X_i^{\{U\}}$ and i=4-6. The rotation matrix ${}^U Rot_{x'''z'''y'''}$ that results from Eq. (13) with the above substitution, is provided by the following relation and for x=x''', y=y''' and z=z''':

$${}^U Rot_{xzy} = \begin{bmatrix} c\Delta\theta_{Cy}c\Delta\theta_{Cz} & s\Delta\theta_{Cx}s\Delta\theta_{Cy} - c\Delta\theta_{Cx}c\Delta\theta_{Cy}s\Delta\theta_{Cz} & c\Delta\theta_{Cx}s\Delta\theta_{Cy} + s\Delta\theta_{Cx}c\Delta\theta_{Cy}s\Delta\theta_{Cz} & 0 \\ s\Delta\theta_{Cz} & c\Delta\theta_{Cx}c\Delta\theta_{Cz} & -s\Delta\theta_{Cx}c\Delta\theta_{Cz} & 0 \\ -s\Delta\theta_{Cy}c\Delta\theta_{Cz} & s\Delta\theta_{Cx}c\Delta\theta_{Cy} + c\Delta\theta_{Cx}s\Delta\theta_{Cy}s\Delta\theta_{Cz} & c\Delta\theta_{Cx}c\Delta\theta_{Cy} - s\Delta\theta_{Cx}s\Delta\theta_{Cy}s\Delta\theta_{Cz} & 0 \\ 0 & 0 & 0 & 1 \end{bmatrix} \tag{20}$$

where c=cos and s=sin.

According to Eq. (11), for $x_i = x_i'$, $y_i = y_i'$, $z_i = z_i'$ with i=4–6, the plane equation of E_2' is defined, which results in the general form of Eq. (16), for i=2.

7. The laser beam axis represented by the linear segment (P_3P_4) impinges on plane E_2' at point P_5. The position vector of point P_5, ${}^U\overrightarrow{p}_{P_5}$, is provided by Eqs. (17), (18), for i=3, j=2 and k=4.
8. The impinging point, P_7, of the laser beam axis on the third (processing) plane, is calculated through the position vector of point P_6 that belongs to the reflecting vector, $\overrightarrow{r}_2$. Point P_6 is provided by the unit vector $\hat{n}_2'$ of the normal vector $\overrightarrow{n}_2' = \left[a_2' \; b_2' \; c_2'\right]^T$, from Eq. (19), for i=3 and j=2.
9. The laser beam axis represented by the linear segment (P_5P_6) impinges on plane E_3 at point P_7. The position vector of point P_7, ${}^U\overrightarrow{p}_{P_7}$, is provided by Eqs. (17), (18), for i=5, j=3, k=7 and x'=x, y'=y and z'=z.
10. The requested angle, ϕ, is the supplementary angle of angle, $\theta_{3,imp.}$ between the vector $\overrightarrow{P_5P_6}$ and the normal vector $\overrightarrow{n}_3 = [a_3 \; b_3 \; c_3]^T$ of plane E_3:

$$\phi = \frac{\pi}{2} - \theta_{3,imp.} = \frac{\pi}{2} - \cos^{-1}\left(\frac{\overrightarrow{P_5P_6} \cdot \overrightarrow{n}_3}{\left|\overrightarrow{P_5P_6}\right|\left|\overrightarrow{n}_3\right|}\right) \tag{21}$$

11. Point P_8 is the projection of point P_5 onto the processing plane E_3. The coordinates of point P_8 $(x_{P_8}, y_{P_8}, z_{P_8})$ are calculated through the parallelism among the vectors $\overrightarrow{P_5P_8}$ and $\overrightarrow{n}_3$ and the fact that point P_8 belongs to plane E_3, for i=5 and j=8:

$$\left.\begin{aligned} \overrightarrow{P_iP_j} \times \overrightarrow{n}_3 &= \begin{vmatrix} \hat{i} & \hat{j} & \hat{k} \\ x_{P_j} - x_{P_i} & y_{P_j} - y_{P_i} & z_{P_j} - z_{P_i} \\ a_3 & b_3 & c_3 \end{vmatrix} = \overrightarrow{0} \\ a_3 x_{P_j} + b_3 y_{P_j} + c_3 z_{P_j} + d_3 &= 0 \\ \Rightarrow x_{P_j} &= \frac{a_3}{b_3}\left(y_{P_j} - y_{P_i}\right) + x_{P_i} \end{aligned}\right\} \tag{22}$$

$$y_{P_j} = \frac{b_3}{a_3^2 + b_3^2 + c_3^2}\left[-a_3 x_{P_i} + \left(\frac{a_3^2 + c_3^2}{b_3}\right) y_{P_i} - c_3 z_{P_i} - d_3\right] \tag{23}$$

$$z_{P_j} = \frac{c_3}{b_3}\left(y_{P_j} - y_{P_i}\right) + z_{P_i} \tag{24}$$

12. Point P_9 is defined as the endpoint of the unit vector, $\hat{i}^{\{4\}} = [1 \quad 0 \quad 0]^T$, along the $x^{\{4\}}$ axis of {D}, and its position vector, ${}^U\overrightarrow{p}_{P_9}$ is provided through the transformation matrix of Eq. (14), for l=D.
13. Point P_{10} is defined as the projection of point P_9 onto the processing plane E_3. The coordinates of point P_{10} $(x_{P_{10}}, y_{P_{10}}, z_{P_{10}})$ are calculated through the parallelism among the vectors $\overrightarrow{P_9P_{10}}$ and $\overrightarrow{n}_3$ and the fact that point P_{10} belongs to plane E_3, according to Eqs. (22), (23), (24), for i=9 and j=10.
14. The orientation angle, ω, is defined by the dot product of vector $\overrightarrow{P_8P_7}$ with vector $\overrightarrow{P_8P_{10}}$.

$$\omega = \cos^{-1}\left(\frac{\overrightarrow{P_8P_7} \cdot \overrightarrow{P_8P_{10}}}{\left|\overrightarrow{P_8P_7}\right|\left|\overrightarrow{P_8P_{10}}\right|}\right) \tag{25}$$

References

1. Macken J (1996) Remote laser welding. IBEC '96 Advanced Technologies & Processes, pp 11–15
2. Highly Efficient & Flexible Remote Welding Systems for Advanced Welded Structures-REMOWELD project, G1RD-2000-00332, 2001–2003
3. Chryssolouris G (1991) Laser machining—theory and practice. Springer, Berlin Heidelberg New York
4. Goebel G, Havrilla D, Wetzig A, Beyer E (2000) Laser welding with long focal length optics. ICALEO A/28–37
5. Rath W, Lingner M (2002) Remote laser welding system using slab laser technology: process data and technical applications. Proceedings of the 10th annual automotive laser applications workshop, March 12–13/2002, MI, USA, 119–127
6. Klotzbach A, Morgenthal L, Schwarz T, Fleischer V, Beyer E (2001) Laser welding on the fly with coupled axes systems. ICALEO, Jacksonville, Florida, USA
7. Beyer E, Klotzbach A, Fleischer V, Morgenthal L (2003) Nd: YAG remote welding with robots. Proceedings of the second international WLT-conference on laser in manufacturing 2003, Munich, June, pp 367–373
8. Belforte DA (2002) Remote welding: industrial laser solutions. July, 15–18
9. Menin R (2002) Remote laser welding. The COMAU solution. Proceedings of the 10th annual automotive laser applications workshop. March 12–13/2002, MI, USA, pp 101–116
10. Tsoukantas G, Salonitis S, Stavropoulos P, Chryssolouris G (2003) An overview of 3D laser materials' processing concepts. 3rd GR-I International Conference on New Laser Technologies and Applications, Proceedings of SPIE, vol. 5131, pp 224–228
11. Leong KH, Geyger HK, Sabo KR, Sanders PG (1997) Threshold laser beam irradiances for melting and welding. J Laser Appl 9:227–231
12. Yue TM, Jiang CY, Xu JH, Lau WS (1996) Laser fantasy: from machining to welding. J Mater Process Technol 57:316–319
13. Tsoukantas G, Chryssolouris G (2006) Theoretical and experimental analysis of the remote welding process on thin, lap-joined AISI 304 sheets. (submitted for publication)